

# Effects of dynamo magnetic fields on observational properties of accreting millisecond X-ray pulsars

Dugasa Belay Zeleke, Solomon Belay Tessema and Seblu Humne Negu

Ethiopian Space Science and Technology Institute (ESSTI), Entoto Observatory and Research Center (EORC), Astronomy and Astrophysics Research and Development Department, P. O. Box 33679 Addis Ababa, Ethiopia; [dugasa32@gmail.com](mailto:dugasa32@gmail.com), [tessemabelay@gmail.com](mailto:tessemabelay@gmail.com), [seblu1557@gmail.com](mailto:seblu1557@gmail.com)

Received 2020 February 4; accepted 2020 July 2

**Abstract** In this paper, we have investigated accreting millisecond X-ray pulsars, which are rapidly rotating neutron stars in low-mass X-ray binaries. These systems exhibit coherent X-ray pulsations that arise when the accretion flow is magnetically channeled to the stellar surface. Here, we have developed the fundamental equations for an accretion disk around accreting millisecond X-ray pulsars in the presence of a dynamo generated magnetic field in the inner part of the disk. We have also formulated the numerical method for the structure equations in the inner region of the disk and the highest accretion rate is enough to form the inner region of the disk, which is overpowered by radiation pressure and electron scattering. Finally, we have examined our results with the effects of dynamo magnetic fields on accreting millisecond X-ray pulsars.

**Key words:** Accretion disk — neutron stars, pulsars — millisecond X-ray pulsars

## 1 INTRODUCTION

Low-mass X-ray binaries (LMXBs) consist of accreting millisecond X-ray pulsars (AMXPs). Such systems arise from a low mass evolved star (a degenerate dwarf star) orbiting a rapidly rotating neutron star (NS). Hence, AMXPs are distinguished from the group of ordinary rotation-powered pulsars by their small spin periods (Becker 2001). In these systems, the accreting matter may spin up the NS. Here, one of the possible endpoints of the evolution of an LMXB is expected to be a millisecond pulsar (Strohmayer 2001). Most LMXBs do not show coherent pulsation in their light curves, an aspect that is still under debate; it could be due to the effect of alignment of the magnetic field on the NS with respect to its rotational axis. The only subclass of LMXBs in which coherent pulsations have been observed is AMXPs.

A more observationally inclined review of an accreting millisecond pulsar is given by Wijnands et al. (2005). It is a transient system in which the outburst stage is associated with matter falling onto the NS surface, which spins up its period on the order of a millisecond. Also, the first real AMXPs were studied by Wijnands & van der Klis (1998), in which the spin frequencies range from 182 up to 599 Hz (Falanga et al. 2013). Among these, the

fastest AXMP is IGR J0029+5934 with a period of just 1.67 ms (Shaw et al. 2005; Falanga et al. 2005). It manifests pulse frequency variations. These observations are very important for understanding of the evolution of NSs in LMXBs (Poutanen 2006).

Here, in AMXPs, we have considered that a rapidly rotating NS has weaker magnetic dipole moments of  $\sim 10^{15} \text{ Tm}^3$  in the inner region than ordinary X-ray pulsars. In these systems, the accretion disk will be extended near the NS and the temperature becomes more so that its opacity can be overpowered by radiation pressure and electron scattering (Lasota 2016). Such magnetic fields are important for transporting angular momentum in these systems. As was studied by Tessema & Torkelsson (2010), the region of the accretion disk which is located in the inner part of corotation radius supplies spin-up torque to the NS while the outer part of the accretion disk brakes the NS. The resultant torque is investigated by the inner region of the disk position, which is displaced inwards as the accretion rate increases.

AMXPs have become important in many areas of astrophysical research. They show a very high average mass transfer rate  $\dot{M} = 10^{14} \text{ kg s}^{-1}$  in the inner region and exhibit persistent X-ray pulsations with less than 10 ms and weak magnetic fields. Many authors

have studied the accretion disk in different models, for example [Shakura & Sunyaev \(1973\)](#); [Ghosh & Lamb \(1979\)](#). Hence, they did not address an accretion disk in these systems, particularly in the inner region of the disk. However, [Tessema & Torkelsson \(2010\)](#) examined the accretion disk around magnetized stars employing pure models of magnetohydrodynamics, but the present study will focus on the accretion disk in AMXPs in the inner region of the disk using analytical and numerical solutions.

In this study, we develop the fundamental equations of an accretion disk with a dynamo that generates an accretion disk around AMXPs, in particular we investigate the solution of these equations in the inner part of the disk incorporating surface density, temperature and radial velocity as a function of the radius, and finally, we present the numerical solution for the structure equations in the inner region of the disk.

This paper is organized as follows: In Section 2 we investigate the fundamental equations of an accretion disk and we present the numerical method for analyzing the structure equation in the inner region of the disk. The associated results and discussion are presented in Section 3 and, finally, we summarize our results in Section 4.

## 2 FUNDAMENTAL EQUATIONS OF AN ACCRETION DISK

### 2.1 Basic Assumptions

In this study, we consider the accretion disk around an AMXP with an NS with mass  $1.4 M_{\odot}$ , radius 10 km and magnetic dipole moment  $10^{15} \text{ Tm}^3$ .

Here, we have considered that the scale height of the disk,  $H$ , is much smaller than the radial extension of the disk,  $R$ , ([Shakura & Sunyaev 1973](#)). The gas in the disk rotates at Keplerian velocity and the orbital kinetic energy is transformed into radiation by viscosity in the accretion disk,  $v$ , while the angular momentum is transported outward.

$$v = \alpha_{ss} c_s H, \quad (1)$$

where  $\alpha_{ss} \sim 10^{-2}$  is turbulent stress in the disk that describes the transport of angular momentum, consistent with numerical simulations suggested by [Hawley et al. \(1995\)](#), and  $c_s$  is the speed of sound in the gas.

### 2.2 Conservation of Mass

The law of conservation of mass or principle of mass conservation states that for any system closed to all transfers of matter and energy, the mass of the system must remain constant over time, as the system's mass cannot change, so the quantity cannot be added nor removed.

Hence, the quantity of mass is conserved over time. Then, conservation of mass is ensured by the continuity equation

$$\frac{\partial \rho}{\partial t} + \nabla \cdot (\rho v) = 0. \quad (2)$$

Then, from Equation (2) we have

$$\nabla \cdot (\rho v) = 0, \quad (3)$$

due to the steady-state condition and where  $\rho$  is the density and  $v = (v_R, v_\phi, v_z)$  of the systems. Here, from the axisymmetric disk we have

$$\frac{1}{R} \frac{\partial}{\partial R} (R \Sigma v_R) = 0, \quad (4)$$

where  $\Sigma$  is the surface density and for a steady state, Equation (4) yields an accretion rate of

$$\dot{M} = -2\pi R \Sigma v_R = \text{constant}. \quad (5)$$

### 2.3 Angular Momentum Conservation

Assuming a steady-state situation, the Navier-Stokes equation can be expressed as

$$\rho(v \cdot \nabla)v = -\nabla p + \rho \nabla \phi + J \times B + \nabla \cdot (\rho v (\nabla v - \frac{2}{3}(\nabla \cdot v))), \quad (6)$$

where  $p$  is pressure,  $v$  kinematic viscosity,  $\phi$  the gravitational potential,  $J = \frac{1}{\mu_0}(\nabla \times B) = (J_R, J_\phi, J_z)$  is the current density and  $B = (B_R, B_\phi, B_z)$  is the magnetic field. Here, we only consider the azimuthal component of the Navier-Stokes equation, which is given by

$$\Sigma \left( \frac{\partial v_\phi}{\partial t} + \frac{v_R}{R} \frac{\partial}{\partial R} (R B_\phi) \right) = \frac{B_R}{\mu_0} \frac{1}{R} \frac{\partial}{\partial R} (R B_\phi) + \frac{B_z}{\mu_0} \frac{\partial B_\phi}{\partial z} + \frac{1}{R^2} \frac{\partial}{\partial R} \left( R^3 \Sigma v \frac{\partial}{\partial R} \left( \frac{v_\phi}{R} \right) \right). \quad (7)$$

Here, we neglect  $\frac{B_R}{R} \frac{\partial}{\partial R} (R B_\phi)$  and for a steady-state disk  $\frac{\partial}{\partial t} = 0$ . By integrating Equation (7) and multiplying both sides by  $R$  ([Tessema & Torkelsson 2010](#)), we get the angular momentum conservation

$$\Sigma \left( v_R \frac{dl}{dR} \right) = \left[ \frac{B_z B_\phi}{\mu_0} \right]_{-H}^H R + \frac{1}{R} \frac{d}{dR} \left[ R^3 v \Sigma \frac{d}{dR} \left( \frac{l}{R^2} \right) \right], \quad (8)$$

where  $l = R v_\phi \propto R^{1/2}$  is the specific angular momentum. Then, the magnetic field of the NS in [Wang \(1995\)](#) is defined by

$$B_z = -\frac{\mu}{R^3}, \quad (9)$$

where  $\mu$  is the magnetic dipole moment. Here, from Equation (8) we have two sources of magnetic fields,  $B_\phi$ , shear magnetic field,  $B_{\phi, \text{shear}}$  and dynamo generated magnetic field,  $B_{\phi, \text{dyn}}$  ([Balbus & Hawley 1998](#)). As was proposed by [Wang \(1995\)](#), the magnetosphere is nearly

force free, and reconnection takes place outside the disk. The ratio of vertical and azimuthal field strengths is related to the shear between the disk and the magnetic field. Then, this ratio can be expressed in the form of Livio & Pringle (1992)

$$\frac{B_{\phi, \text{shear}}}{B_z} \sim -\gamma \left( \frac{\Omega_k - \Omega_s}{\Omega_k} \right), \quad (10)$$

where  $\Omega_k$  and  $\Omega_s$  represent the Keplerian angular velocity at the inner radius of the disk and the angular velocity of the star, respectively. The subscript  $k$  denotes the Keplerian situation. By rearranging Equation (10), we obtain

$$B_{\phi, \text{shear}} = -\gamma B_z \left( \frac{\Omega_k - \Omega_s}{\Omega_k} \right), \quad (11)$$

where  $\gamma$  is a dimensionless parameter of the system (Ghosh & Lamb 1979). The dynamo magnetic field,  $B_{\text{dyn}}$ , generated by magnetohydrodynamical turbulence in an accretion disk through the dynamo action (Balbus & Hawley 1998) is written as

$$B_{\phi, \text{dyn}} = \epsilon (\alpha_{ss} \mu_0 \gamma_{\text{dyn}} P(r))^{1/2}, \quad (12)$$

where the subscript dyn stands for the dynamo generated magnetic field and  $P(r)$  is the radiation pressure. From Equation (12),  $\gamma_{\text{dyn}}$  is the order of 10 as asserted by Brandenburg et al. (1995) and  $\epsilon$  is a dynamo parameter that describes the direction of the magnetic field in the range of  $-1 \leq \epsilon \leq 1$ . Then, substituting Equations (9), (11) and (12) into Equation (8) and from Tessema & Torkelsson (2010) we obtain

$$\begin{aligned} \Sigma \left( v_R \frac{dl}{dR} \right) &= 2\epsilon \frac{(\mu R^{-3})}{\mu_0} (\alpha_{ss} \mu_0 \gamma_{\text{dyn}} P(r))^{1/2} R \\ &- 2\gamma \frac{(\mu R^{-3})^2}{\mu_0} \left( \frac{\Omega_k - \Omega_s}{\Omega_k} \right) R \\ &+ \frac{1}{R} \frac{d}{dR} \left( R^3 v \Sigma \frac{d}{dR} \left( \frac{l}{R^2} \right) \right). \end{aligned} \quad (13)$$

Equation (13) represents an ordinary differential equation for an accretion disk with angular momentum conservation.

## 2.4 Hydrostatic Vertical Balance

We now consider the structure of the disk in the vertical  $z$ -direction. Hence, the angular momentum conservation is reduced to hydrostatic equilibrium condition if the net flow of gas along the vertical direction is zero. Then, the hydrostatic equilibrium equation is defined as

$$\frac{1}{\rho} \frac{\partial P}{\partial z} = \frac{\partial}{\partial z} \left( \frac{GM}{(R^2 + z^2)} \right)^{1/2}, \quad (14)$$

in the limit  $z \ll R$  and neglecting the self-gravity of the disk, Equation (14) becomes

$$\frac{1}{\rho} \frac{\partial P}{\partial z} = -\frac{GMz}{R^3}, \quad (15)$$

where  $G$  and  $M$  are the universal gravitational constant and mass of the accreting star, respectively.

As a consequence, from Equation (1) and the approximation of vertical pressure gradient, we express  $\frac{\partial P}{\partial z} \sim \frac{P}{H}$  and  $z \sim H$ . Then, Equation (15) yields

$$\frac{P}{\rho} = c_s^2. \quad (16)$$

Thus, from Equation (15) and Equation (16) we find  $H$  as

$$H \cong c_s R \left( \frac{R}{GM} \right)^{1/2}. \quad (17)$$

For a thin accretion disk, the local Kepler velocity should be highly supersonic. In general, we can define a central disk density approximately by

$$\rho = \frac{\Sigma}{H} \quad \text{and} \quad H = c_s \left( \frac{R}{v_\phi} \right), \quad (18)$$

where  $v_\phi$  is given by

$$v_\phi = \sqrt{\left( \frac{GM}{R} \right)}. \quad (19)$$

The speed of sound can be expressed by utilizing Equation (18) and (19) as

$$c_s = \frac{H}{R} \left( \frac{GM}{R} \right)^{1/2}. \quad (20)$$

As was proposed by Tessema & Torkelsson (2010), we can write the gas and radiation pressure as

$$P = \frac{\rho K_B T_c}{\bar{\mu} m_p} + \frac{4\sigma}{3c} T_c^4, \quad (21)$$

where  $\sigma$  is the Stefan-Boltzmann constant,  $m_p$  is the mass of a proton,  $T_c^4$  central temperature, the subscript  $c$  signifies values in the central plane,  $c$  is the speed of light,  $\bar{\mu}$  is the mean molecular weight for ionized gas and  $K_B$  is Boltzmann's constant. Then, we can write the pressure for hydrostatic equilibrium applying Equations (15) and (18) as

$$P = \Sigma \left( \frac{HGM}{R^3} \right). \quad (22)$$

Here, for a Newtonian accretion disk, the  $f_{R\phi}$  component of the viscous stress tensor is given by

$$f_{R\phi} = \frac{-3}{2} \rho v \Omega = \alpha_{ss} P(r), \quad (23)$$

where

$$\Omega = \left( \frac{GM}{R^3} \right)^{\frac{1}{2}}. \quad (24)$$

Substituting Equation (24) into Equation (23) we obtain

$$f_{R\phi} = \frac{-3}{2} \rho v \left( \frac{GM}{R^3} \right)^{\frac{1}{2}} = \alpha_{ss} P(r), \quad (25)$$

where  $\rho = \frac{\Sigma}{2H}$ . Then, the viscous stress tensor,  $f_{R\phi}$ , can be written as

$$f_{R\phi} = \frac{3\Sigma v}{4H} \left( \frac{GM}{R^3} \right)^{1/2} = \alpha_{ss} P(r). \quad (26)$$

From Equations (16), (22) and (26) we obtain the gas density of the NS as

$$\rho = \frac{3v\Sigma}{4\alpha_{ss}H^3} \left( \frac{GM}{R^3} \right)^{-1/2}. \quad (27)$$

Also, we can express the scale height of the disk in terms of the total pressure as

$$H = \left( \frac{\rho k_B T_c R^3}{m_p \bar{\mu} GM} + \frac{4\sigma T_c^4 R^3}{3c\rho GM} \right)^{1/2}. \quad (28)$$

The local viscous dissipation is determined by radiative losses when the matter flow through an optical disk is low. Then, we have the  $T_c$ ,  $v$ ,  $\Sigma$ ,  $M$  and  $R$  relation

$$\frac{4\sigma}{3\tau} T_c^4 = \frac{9}{8} v \Sigma \frac{GM}{R^3}. \quad (29)$$

Here, the optical depth of the disk,  $\tau$ , is given by

$$\tau = \int_0^H k_R \rho dz = \rho H k_R, \quad (30)$$

where  $K_R = k_{es} + k_{ff}$ . In the inner region of the disk, the temperature is high and the approximation of  $k_R \approx k_{es}$  is valid because this region is dominated by electron scattering opacity. Then, from Equations (29) and (30) we obtain the central temperature

$$T_c^4 = \frac{27}{32\sigma} v \Sigma^2 k_R \frac{GM}{R^3}. \quad (31)$$

As was investigated by Tessema & Torkelsson (2010); Frank et al. (2002); Shapiro et al. (1983):

$$R_A = \left( \frac{2\pi^2 \mu^4}{GM M^2 \mu_0^2} \right)^{\frac{1}{7}} \simeq 1.4 \times 10^4 \dot{M}_{14}^{-\frac{2}{7}} M_1^{-\frac{1}{7}} \mu_{15}^{\frac{4}{7}} m, \quad (32)$$

$$R_{co} = \left( \frac{GM P_{\text{spin}}^2}{4\pi^2} \right)^{\frac{1}{3}} \simeq 1.5 \times 10^6 P_{\text{spin}}^{\frac{2}{3}} M_1^{\frac{1}{3}} m, \quad (33)$$

where  $P_{\text{spin}} = \frac{2\pi}{\Omega_s}$  and  $M_1 = \frac{M}{M_\odot}$ . Let us to introduce a parameter  $y = \Sigma v$  in order to solve an ordinary differential

equation for an accretion disk. Then, from Equations (13), (22), (27), (32) and (33), we have

$$y' = \frac{\dot{M}}{6\pi r} - \frac{y}{2r} - \epsilon D_1 (GM)^{-\frac{1}{4}} R_A^{-\frac{3}{4}} - D_2 R_A^{-\frac{9}{2}} \left[ 1 - \left( \frac{R_A}{R_{co}} \right)^{\frac{3}{2}} \right]. \quad (34)$$

where,

$$D_1 = \sqrt{\left( \frac{4\mu^2 \gamma_{\text{dyn}} y}{3\mu_0 H R_A^{3/2}} \right)} \quad \text{and} \quad D_2 = \frac{4\mu^2 \gamma}{3\mu_0 (GM)^{1/2}}, \quad (35)$$

which is a differential equation of  $y$  for an accretion disk around an AMXP. At large radii, the solution of Equation (34) approaches the Shakura-Sunyaev solution, which gives us the boundary condition  $y \rightarrow \Lambda \dot{M}$  as  $R \rightarrow \infty$ . Here, we need to transform Equation (34) by introducing dimensionless quantities  $\Lambda$  and  $r$ , so that

$$y = \Lambda \dot{M} \quad (36)$$

where  $\Lambda$  is a dimensionless parameter for the accretion disk and

$$R = r R_A. \quad (37)$$

Here  $r$  is a dimensionless radial coordinate and  $R_A$  is the Alfvén radius, which is a characteristic radius at which magnetic stresses dominate the flow in the accretion disk.

As noted by Elsner & Lamb (1977), we have  $\omega_s$  as

$$\omega_s = \left( \frac{R_A}{R_c} \right)^{\frac{3}{2}} = 0.36 M_1^{-\frac{5}{7}} \dot{M}_{14}^{-\frac{3}{7}} \mu_{15}^{\frac{6}{7}} \left( \frac{P_{\text{spin}}}{4.8 \text{ ms}} \right)^{-1}. \quad (38)$$

Finally, using Equation (36), Equation (37) and Equation (38) we get the differential equation of an accretion disk from Equation (34) which is given by

$$\Lambda' = \frac{1}{6\pi r} - \frac{\Lambda}{2r} - \epsilon D_3 (GM)^{-\frac{1}{4}} R_A^{-\frac{5}{4}} r^{-\frac{9}{4}} - D_4 r^{-\frac{9}{2}} \left( 1 - \omega_s r^{\frac{3}{2}} \right). \quad (39)$$

where  $D_3 = \sqrt{\left( \frac{4\mu^2 \gamma_{\text{dyn}} \Lambda}{3\mu_0 H M} \right)}$  and  $D_4 = \frac{4\mu^2 \gamma}{3\mu_0 (GM)^{\frac{1}{2}} M} R_A^{-\frac{7}{2}}$ . This equation is the new analytical solution for an accretion disk around an AMXP.

## 2.5 The Structure of the Disk

Here, to analyze the dynamics of an accretion disk, we examine the inner region of the disk, in which the radiation pressure is much higher than the gas pressure and the accretion rate is large. In this region, Compton scattering occurs more frequently than free-free absorption. To solve Equation (39) numerically, we have to determine scale height in the inner region of the disk, which is defined by

$$H = \frac{9}{8c} k_{es} (\dot{M} \Lambda). \quad (40)$$

Then, the shear magnetic field is expressed as

$$B_{\phi, \text{shear}} = -4 \times 10^3 \gamma M_1^{\frac{3}{7}} \dot{M}_{14}^{\frac{6}{7}} \mu_{15}^{\frac{-5}{7}} \left(1 - \omega_s r^{\frac{3}{2}}\right) r^{-3} T. \quad (41)$$

In the inner region of the disk, the radiation pressure is larger than the gas pressure, and we have that:

$$\Sigma = 9.57 \times 10^1 \alpha_{ss}^- M_1^{-5/7} \dot{M}_{14}^{-10/7} \mu_{15}^{6/7} \Lambda(r)^{-1} r^{3/2} \text{ kg m}^{-2}, \quad (42)$$

$$\rho_c = 3.18 \times 10^{-2} \alpha_{ss}^- M_1^{-5/7} \dot{M}_{14}^{-17/7} \mu_{15}^{6/7} \Lambda(r)^{-2} r^{3/2} \text{ kg m}^{-3}, \quad (43)$$

$$v_R = 1.18 \times 10^7 \alpha_{ss} M_1^{6/7} \dot{M}_{14}^{19/7} \mu_{15}^{-10/7} \Lambda(r) r^{-5/2} \text{ m s}^{-1}, \quad (44)$$

$$T_c = 1.86 \times 10^6 \alpha_{ss}^{-1/4} M_1^{5/28} \dot{M}_{14}^{3/28} \mu_{15}^{-3/4} r^{-3/8} \text{ k}, \quad (45)$$

$$v = 1.1 \times 10^{12} \alpha_{ss} M_1^{5/7} \dot{M}_{14}^{17/7} \mu_{15}^{-6/7} \Lambda(r)^2 r^{-3/2} \text{ m}^2 \text{ s}^{-1}, \quad (46)$$

$$\tau_{es} = 1.86 \alpha_{ss}^{-1} M_1^{-5/7} \dot{M}_{14}^{-10/7} \mu_{15}^{6/7} \Lambda(r)^{-1} r^{3/2}. \quad (47)$$

The transition radius in the inner region of the disk is estimated by approximating  $\Lambda = 1/3\pi$ .

$$r_{IM} = 12.5 \mu_{15}^{8/21} \alpha_{ss}^{2/21} M_1^{10/21} \dot{M}_{14}^{22/21} \mu_{15}^{-4/7}. \quad (48)$$

Here, the accretion disk outside of the Alfvén radius is overpowered by radiation pressure only if

$$\mu_{15} < 82.56 \mu_{15}^{2/3} \alpha_{ss}^{-1/16} M_1^{5/6} \dot{M}_{14}^{11/6}. \quad (49)$$

This circumstance is not satisfied for an ordinary X-ray pulsar with a magnetic dipole moment of  $\sim 10^{20} \text{ Tm}^3$  (White & Stella 1988), though it can be satisfied for AMXPs.

So far, we have incorporated equations of an accretion disk around AMXPs, then we applied some parameters and investigated Equation (39) in the inner region of the disk. The inner region is where the radiation pressure is overpowered and electron scattering is the most important source of opacity (Shakura & Sunyaev 1973). As a result, in the innermost regions, the emitted spectrum of the disk cannot be approximated by a blackbody spectrum. Whereas if the accretion rates are high, radiation pressure towards the inner edge of the accretion disk exceeds the thermal pressure. Using the appropriate selection of the magnetic field and accretion rate, then the inner region solution is found below.

### 3 RESULT AND DISCUSSION

#### 3.1 Global Solutions

Here, as was studied by Tessema & Torkelsson (2011), we integrate Equation (39) for the inner region inwards from very small radius  $\sim 12.5$  and  $\Lambda = 1/3\pi$ . The dimensionless parameters  $\gamma$ ,  $\gamma_{\text{dyn}}$  and  $\alpha_{ss}$  are 1, 10 and

$10^{-2}$ , respectively. Hence, the disk is overpowered by radiation pressure and electron scattering where  $R_A < R_{IM}$  by increasing accretion rate. In this region, it is possible to use the accretion rate up to the Eddington limit, so that we take  $\dot{M} = 1.5 \times 10^{14} \text{ kg s}^{-1}$  for our calculation and we apply  $\Lambda = 1/3\pi$  for the analytical solution of the disk, and solve Equation (39) for the inner region of the disk starting from  $r_{IM} = 12.5$ . Our solutions for the inner disk region of AMXPs with different dynamo parameters such as  $\epsilon = 0.45, 0.15, 0, -0.15$  and  $-0.45$  are shown in Figure 1. This figure depicts the variations of  $\Lambda$  as a function of  $r$  for all  $\epsilon = 0.45, 0.15$  and  $0$ . All solutions are case V inner boundaries except  $-0.15$  and  $-0.45$  (Tessema & Torkelsson 2011).

In Figure 3, the high surface density results in a hot flow. Here, the mid-plane temperature as a function of radius in the inner region of the disk does not depend on  $\Lambda$  so that as the radius decreases the temperature increases.

In Figure 4, we affirm that the high surface density corresponds to a decrease in radial velocity and this radial velocity is dependent on  $\Lambda$ . In this figure, as the inner edge of the accretion disk approaches the surface of the star, the radial velocity either goes to zero or infinity. Here, the radial velocity decreases as the radius increases.

#### 3.2 Accretion Torques

The torques on an NS range from material to magnetic. It is obtained from Equation (13) by multiplying  $2\pi R$  and then integrating from the inner radius of the disk,  $R_{\text{in}}$ , to the outer edge of the disk,  $R_{\text{out}}$ , see, e.g., Kluźniak & Rappaport (2007); Tessema & Torkelsson (2010); Shi et al. (2015).

$$\begin{aligned} & \dot{M} \sqrt{GMR_{\text{in}}} - \dot{M} \sqrt{GMR_{\text{out}}} = \\ & - \int_{R_{\text{in}}}^{R_{\text{out}}} \left[ \frac{4\pi(\mu R^{-3})}{\mu_0} (B_{\phi, \text{dyn}} + B_{\phi, \text{shear}}) \right] R^2 dR \\ & - \left[ 3\pi y (GMR)^{1/2} \right]_{R_{\text{in}}}^{R_{\text{out}}}. \end{aligned} \quad (50)$$

Note that the two expressions on the left hand side of Equation (50) provide the rate at which angular momentum is transported past the inner and outer edges of the accretion disk, while the right hand side shows the implications of magnetic and viscous torques on the angular momentum balance. In this case, the material, magnetic and viscous torque can be expressed in Equations (51), (52), (53), (54), (55) and (56). Thus, the material torque at the inner edge of the disk on the NS is given by

$$N_{\text{in}} = \dot{M} (GMR_{\text{in}})^{1/2} = 1.4 \times 10^{26} \mu_{15}^{2/7} M_1^{3/7} \dot{M}_{14}^{6/7} r_{\text{in}}^{1/2}. \quad (51)$$

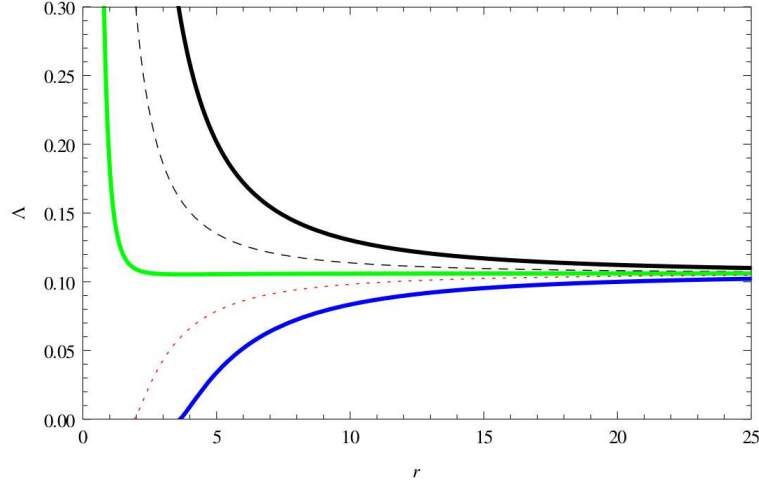


**Fig. 1** Result of  $\Lambda$  as a function of  $r$  for the AMXPs with accretion rate  $M = 1.5 \times 10^{14} \text{ kg s}^{-1}$  and the different dynamo parameters are displayed with  $\epsilon = -0.45$  (solid blue line),  $\epsilon = -0.15$  (red dotted line),  $\epsilon = 0$  (solid green line),  $\epsilon = 0.15$  (black dotted line) and  $\epsilon = 0.45$  (solid black line). In Fig. 2, the  $\Sigma$  is purely a decreasing function of  $r$  for  $\epsilon = 0$  and  $0.45$ , and increasing for  $\epsilon = -0.45$ .

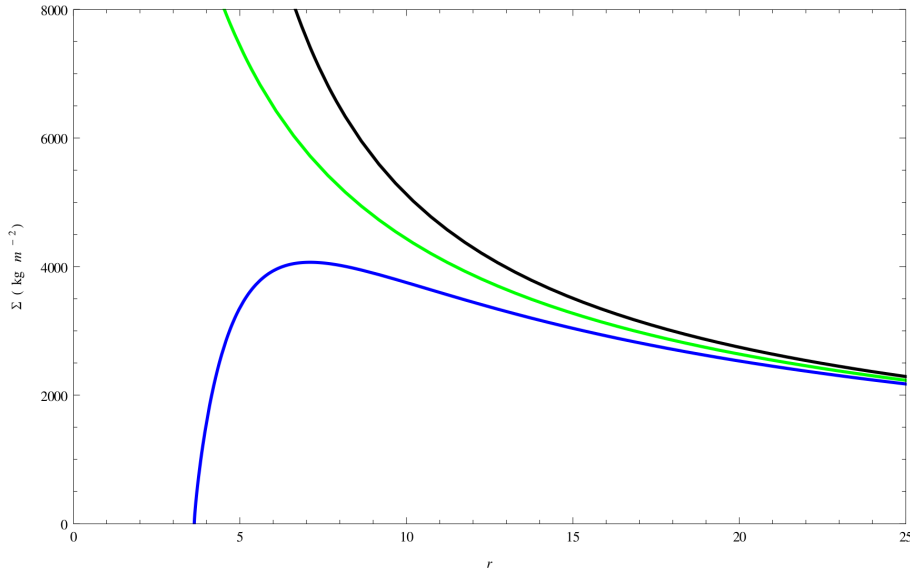


**Fig. 2** Result of  $\Sigma$  as a function of  $r$  for AMXPs with accretion rate  $M = 1.5 \times 10^{14} \text{ kg s}^{-1}$  and the different dynamo parameters are displayed with  $\epsilon = -0.45$  (solid blue line),  $\epsilon = 0$  (solid green line) and  $\epsilon = 0.45$  (solid black line).

Here, in Figure 5 we investigate the inner accretion torque on the disk in the inner region of the disk. This material torque increases as the accretion rate and the inner radius increase.

The magnetic torque is the result of the coupling between the vertical magnetic field of the star and the toroidal magnetic field in the disk. Hence, the torque acting on the lower surface of the disk can be written (Ghosh & Lamb 1979) as

$$N_{\text{mag}} = -4\pi \int_{R_{\text{in}}}^{R_{\text{out}}} \frac{-(\mu R^{-3}) (B_{\phi, \text{dyn}} + B_{\phi, \text{shear}}) R^2 dR}{\mu_0}. \quad (52)$$

This magnetic torque is separated into shear and dynamo generated magnetic torque. Then, the shear magnetic torque,  $N_{\text{mag, shear}}$ , is defined by

$$\begin{aligned} N_{\text{mag, shear}} &= \int_{R_{\text{in}}}^{R_{\text{out}}} 4\pi \frac{-(\mu R^{-3}) B_{\phi, \text{shear}}}{\mu_0} R^2 dR \\ &\approx 4 \times 10^{26} \gamma \mu_{15}^{2/7} M_1^{3/7} \dot{M}_{14}^{6/7} \int_{r_0}^{\infty} [r^{-4} (1 - \omega_s r^{3/2})] dr, \end{aligned} \quad (53)$$

and the dynamo generated magnetic torque on the NS is

$$N_{\text{mag, dyn}} = - \int_{R_{\text{in}}}^{R_{\text{out}}} 4\pi \frac{-(\mu R^{-3}) B_{\phi, \text{dyn}}}{\mu_0} R^2 dR. \quad (54)$$

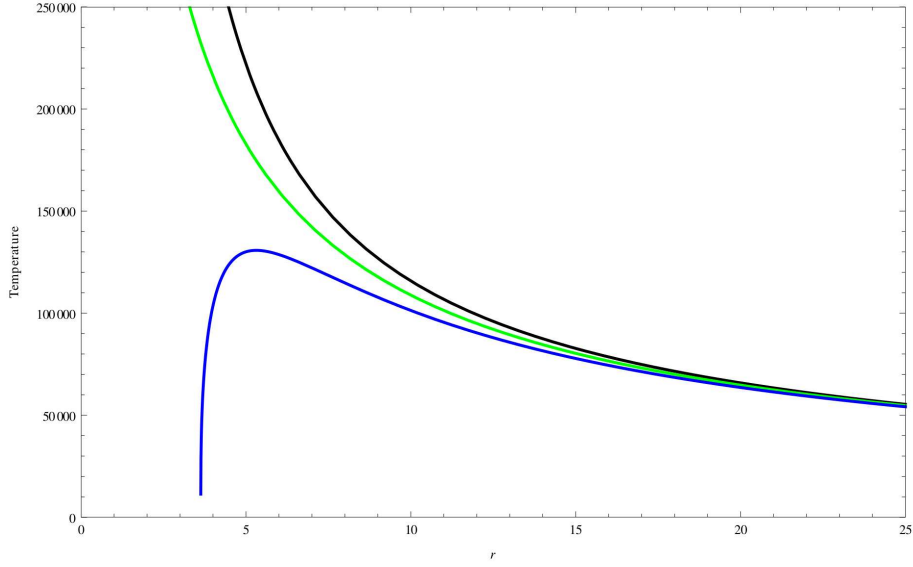


**Fig. 3** Result of  $T_c$  as a function of  $r$  for AMXPs with accretion rate  $\dot{M} = 1.5 \times 10^{14} \text{ kg s}^{-1}$  and the different dynamo parameters are displayed with  $\epsilon = -0.45$  (solid blue line),  $\epsilon = 0$  (solid green line) and  $\epsilon = 0.45$  (solid black line).

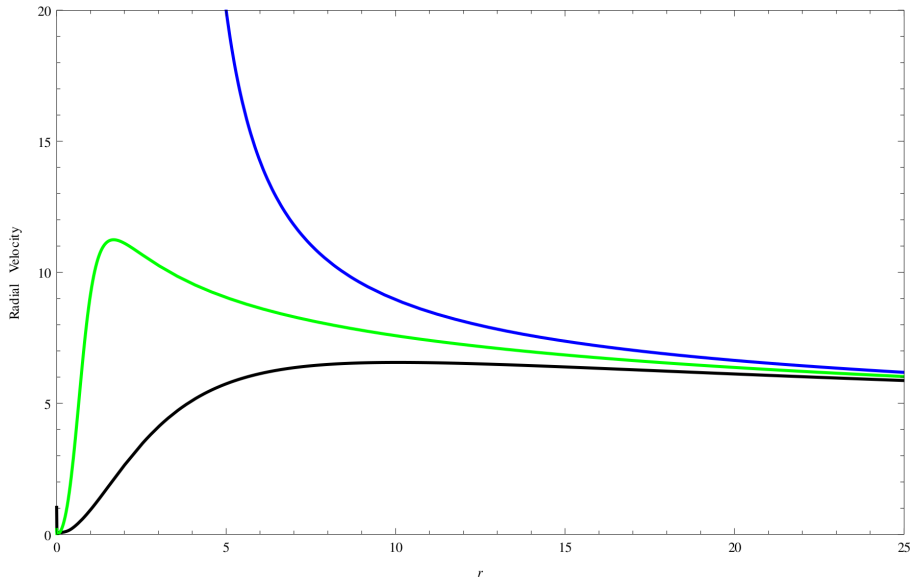


**Fig. 4** Result of  $\bar{V}_R$  as a function of  $r$  for AMXPs with accretion rate  $\dot{M} = 1.5 \times 10^{14} \text{ kg s}^{-1}$  and the different dynamo parameters are displayed with  $\epsilon = -0.45$  (solid blue line),  $\epsilon = 0$  (solid green line) and  $\epsilon = 0.45$  (solid black line).

Here, the dynamo generated magnetic torque in the inner region of the disk is defined by

$$N_{\text{dyn,inner}} = 7 \times 10^{26} \epsilon \gamma_{\text{dyn}}^{1/2} \mu_{15}^{4/7} M_1^{5/14} \dot{M}_{14}^{3/14} \int_{\text{inner}} r^{-7/4} dr. \quad (55)$$

On the other hand, the viscous torque in the inner region of the disk is given by

$$\begin{aligned} N_{\text{vis}} &= -3\pi y R_{\text{in}} (GMR_{\text{in}})^{1/2} \\ &= -1.3 \times 10^{27} \mu_{15}^{2/7} M_1^{3/7} \dot{M}_{14}^{6/7} \Lambda(r_0) r_{\text{in}}^{1/2}. \end{aligned} \quad (56)$$

Moreover, as was investigated by [Tessema & Torkelsson \(2011\)](#), the standard accretion disk solution has a case D inner region boundary when the viscous torque is neglected in accretion disk theory. Hence, the angular momentum is transported from the NS to the disk when it is in the case V inner region boundary.

Except for the case when  $\epsilon = 0$ , the dynamo magnetic torque is importantly greater than the shear magnetic torque, and both are greater for  $\epsilon = 0.15$  than for  $\epsilon = 0.45$ . Because of this effect, the central hole of the disk grows too large when  $\epsilon = 0.45$ . The overpowered torque at  $\epsilon = 0.45$

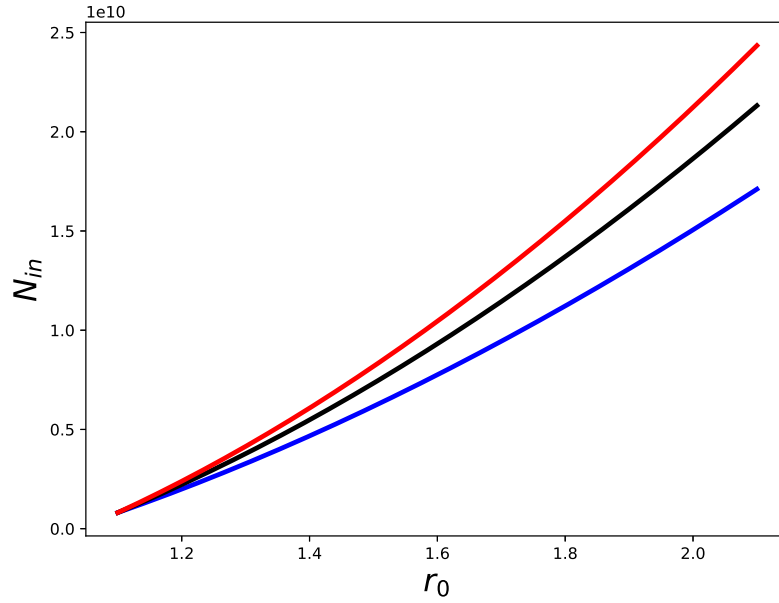


**Fig. 5** This figure plots the material torque on AMXPs with different accretion rates by varying the inner region radius,  $r_{in}$ , of the disk.

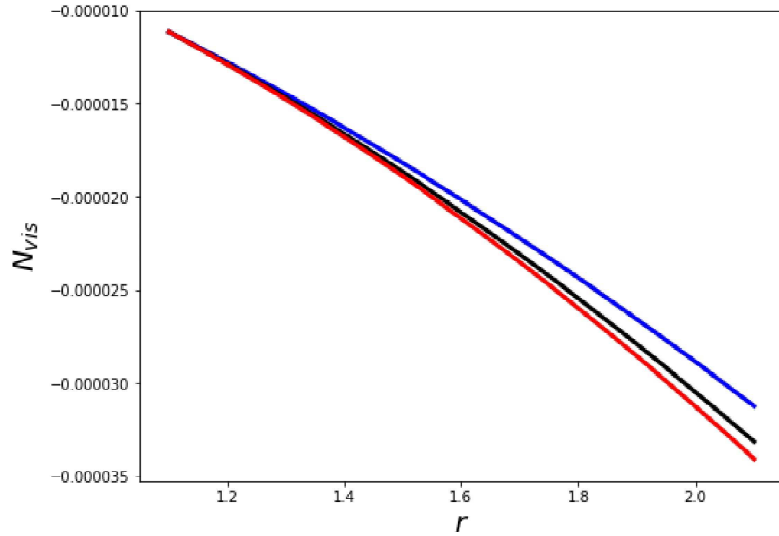


**Fig. 6** This figure plots the variation of viscous torque as a function of radius for AMXPs with different masses and radii in the inner region of the disk.

is the viscous torque in this region, which is ignored as displayed in Figure 6 below.

### 3.3 Comparison with Observational Results

There is a large variation in the accretion rates among AMXPs. The well studied system IGR J00291+5934 is accreting at a rate of at least  $\sim 10^{14} \text{ kg s}^{-1}$  based on its X-ray flux (Burderi et al. 2007), while in some other systems, for instance, SAX J1808.4-3658 (Bildsten & Chakrabarty

2001), the NS is accreting at a rate below  $10^{12} \text{ kg s}^{-1}$  from a brown dwarf companion. There is also great doubt in the spin variations that have been reported for AMXPs. For instance, Burderi et al. (2006) reported  $\dot{\nu}$  for these spin variations between  $-7.6 \times 10^{-14}$  and  $4.4 \times 10^{-13} \text{ Hz s}^{-1}$  for SAX J1808.4-3658, but Hartman et al. (2008) noted that the measurements of this source are plagued by more variations in the pulse shape, and put an upper limit of

$2.5 \times 10^{-14} \text{ Hz s}^{-1}$  on the spin variations and found a long-term spin down of  $\dot{\nu} = -5.6 \times 10^{-16} \text{ Hz s}^{-1}$ .

On the other hand, Burderi et al. (2007) reported that IGR J00291+5934 was spinning up at  $\sim 10^{-12} \text{ Hz s}^{-1}$  during the December 2004 outburst. More spin variations have been observed in some AMXPs that depend on the accreting torque, which is given by

$$N = 2\pi\dot{\nu}I, \quad (57)$$

where  $I$  is  $\text{Kg m}^2$  and  $\dot{\nu}$  is  $\text{Hz s}^{-1}$ .

#### 4 CONCLUSIONS

In this paper, we have studied the interaction between AMXPs and the inner region of the disk, which is supported by the dynamo generated magnetic field. Hence, we found that the fundamental equations of an accretion disk around AMXPs give a more stable system than the previous study. We have made an effort to find an analytical solution by applying a numerical method for an accretion disk around AMXPs in the inner region of the disk, in which the accretion rate is high and the disk is overpowered by radiation pressure and the electron scattering region. Here, the analytical solution of Equation (39) at the higher accretion rate in the inner region of the accretion disk is greater than the radius of the NS for different values of dynamo parameters,  $\epsilon$ , and we observed the behavior of these solutions in the inner region in Figure 1. We have formulated the numerical method for the structure equation in the inner region of the disk and the highest accretion rate is sufficient to make the innermost region of the accretion disk be overpowered by radiation pressure and electron scattering. We have ascertained the relationship between surface density and radius in Figure 2. Then, in this figure, the surface density decreases with radius. The viscous torque in the inner region of the disk is ignored, which is displayed in Figure 6. Hence, the viscous torque on AMXPs decreases for different masses and radii of the accretion disk. The accretion torque is important in explaining the observed variations in the spin frequency of AMXPs like IGR J00291+5934. Thus, we have found that the spin derivatives for accretion rate  $1.5 \times 10^{14} \text{ kg s}^{-1}$  in this model, which are in agreement with RXTE observed data for AMXPs, are consistently explained by this model.

**Acknowledgements** We thank the Ethiopian Space Science and Technology Institute, Entoto Observatory and Research Center and Astronomy and Astrophysics

Research and Development Department for supporting this research. This research has made use of the Astronomical Data system.

#### References

- Balbus, S. A., & Hawley, J. F. 1998, *Reviews of Modern Physics*, 70, 1
- Becker, W. 2001, in *AIPC*, 599, X-ray Astronomy: Stellar Endpoints, AGN, and the Diffuse X-ray Background, eds. N. E. White, G. Malaguti, & G. G. C. Palumbo, 13
- Bildsten, L., & Chakrabarty, D. 2001, *ApJ*, 557, 292
- Brandenburg, A., Nordlund, A., Stein, R. F., & Torkelsson, U. 1995, *ApJ*, 446, 741
- Burderi, L., Di Salvo, T., Menna, M. T., Riggio, A., & Papitto, A. 2006, *ApJL*, 653, L133
- Burderi, L., Di Salvo, T., Lavagetto, G., et al. 2007, *ApJ*, 657, 961
- Elsner, R. F., & Lamb, F. K. 1977, *ApJ*, 215, 897
- Falanga, M., Kuiper, L., Poutanen, J., et al. 2013, arXiv e-prints, arXiv:1302.2843
- Falanga, M., Kuiper, L., Poutanen, J., et al. 2005, *A&A*, 444, 15
- Frank, J., King, A., & Raine, D. J. 2002, *Accretion Power in Astrophysics: Third Edition* (Cambridge, UK: Cambridge Univ. Press)
- Ghosh, P., & Lamb, F. K. 1979, *ApJ*, 234, 296
- Hartman, J. M., Patruno, A., Chakrabarty, D., et al. 2008, *ApJ*, 675, 1468
- Hawley, J. F., Gammie, C. F., & Balbus, S. A. 1995, *ApJ*, 440, 742
- Kluźniak, W., & Rappaport, S. 2007, *ApJ*, 671, 1990
- Lasota, J.-P. 2016, *Astrophysics and Space Science Library*, 440, *Black Hole Accretion Discs*, ed. C. Bambi (Springer-Verlag Berlin Heidelberg), 1
- Livio, M., & Pringle, J. E. 1992, *MNRAS*, 259, 23P
- Poutanen, J. 2006, *Advances in Space Research*, 38, 2697
- Shakura, N. I., & Sunyaev, R. A. 1973, *A&A*, 500, 33
- Shapiro, S. L., Teukolsky, S. A., & Wasserman, I. 1983, *ApJ*, 272, 702
- Shaw, S. E., Mowlavi, N., Rodriguez, J., et al. 2005, *A&A*, 432, L13
- Shi, C.-S., Zhang, S.-N., & Li, X.-D. 2015, *ApJ*, 813, 91
- Strohmayer, T. E. 2001, *ApJL*, 552, L49
- Tessema, S. B., & Torkelsson, U. 2010, *A&A*, 509, A45
- Tessema, S. B., & Torkelsson, U. 2011, *MNRAS*, 412, 1650
- Wang, Y. M. 1995, *ApJL*, 449, L153
- White, N. E., & Stella, L. 1988, *MNRAS*, 231, 325
- Wijnands, R., Homan, J., Heinke, C. O., Miller, J. M., & Lewin, W. H. G. 2005, *ApJ*, 619, 492
- Wijnands, R., & van der Klis, M. 1998, *Nature*, 394, 344